ACS APPLIED MATERIALS & INTERFACES

Research Article

www.acsami.org

Inorganic–Organic p-n Heterojunction Nanotree Arrays for a High-Sensitivity Diode Humidity Sensor

Ke Wang, Xuemin Qian, Liang Zhang, Yongjun Li, and Huibiao Liu*

Beijing National Laboratory for Molecular Science (BNLMS), CAS Key Laboratory of Organic Solids, Institute of Chemistry, Chinese Academy of Sciences, Beijing, 100190, People's Republic of China

Supporting Information

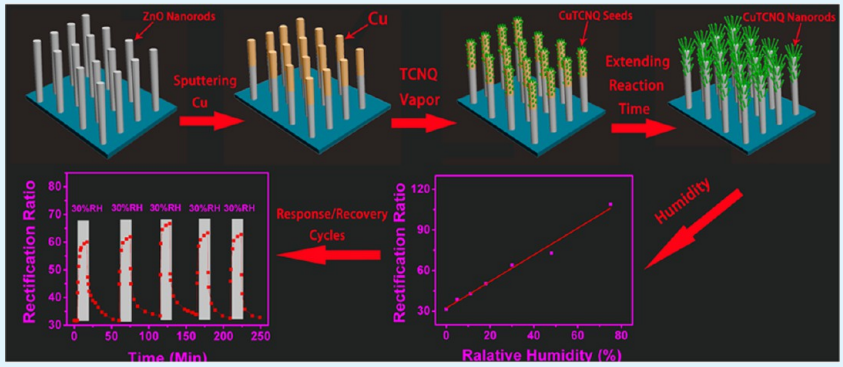

ABSTRACT: Large-area and ordered arrays (16 cm^2) of an inorganic–organic p-n heterojunction nanotree (NT) were successfully fabricated. The nanotree arrays consist of ZnO nanorods (NRs) as backbones and CuTCNQ (TCNQ = 7,7,8,8-tetracyanoquinodimethane) NRs as branches. The sizes of CuTCNQ NRs can be tuned by the thickness of the Cu layer deposited on the surface of ZnO NR. The CuTCNQ/ZnO NT arrays displayed excellent diode nature and obvious size-dependent rectification ratios were observed. Moreover, the CuTCNQ/ZnO NT arrays were first applied for the fabrication of a diode-type humidity sensor, which displayed ultrahigh sensitivity and quick response/recovery properties at room temperature. The detection limitation of this new diode-type humidity sensor lowers to 5% relative humidity (RH).

KEYWORDS: *inorganic–organic p-n heterojunction, 2D ordered aligned arrays, nanotrees, diode, humidity sensor*

1. INTRODUCTION

The ability to manufacture and organize one-dimensional (1D) nanomaterials into ordered two-dimensional (2D) or three-dimensional (3D) macro-size structures is of extreme importance in developing new devices and applications. Macro-size architectures based on 1D nanomaterials (e.g., tubes, wires, rods) provide a platform to integrate nanostructures at a large and controllable scale into high-performanced devices like chemo- and biosensors,[1] photoelectric device, field emitters, field effect transistors, catalysts, and energy applications.[2−10] However, the main research has focused on the carbon nanotubes, 1D inorganic and organic nanomaterials,[11−17] which can be used as active elements in memory, OLED, and photoswitchers, etc.[18−23] Recently, inorganic–organic heterojunction 1D nanomaterials have attracted a great deal of interest because this new class of solid nanomaterials exhibit distinct architectures and properties that their individual components do not have on their nano- and bulk materials due to the synergistic effect.[24] Numerous methods available for the fabrication of inorganic–organic heterojunction nanowires have been devised.[25−31] Up until now, 2D ordered aligned heterojunction nanowires are achieved only by template methods.[25,27−30]However, removal of the templates can lead to collapse or entanglement of the aligned nanowires. Especially, the area of 2D ordered aligned heterojunction nanowires is restricted by the size of the template. As far as we know, there are not any available methods to fabricate large-area inorganic–organic heterojunction hierarchical nanostructure arrays without a template. Therefore, developing new methods to fabricate large-area 2D ordered aligned inorganic–organic heterojunction nanostructure arrays is still a great challenge.

ZnO is a typical n-type inorganic semiconductor, which has been extensively researched on their optoelectronic, optical, and electrical properties.[32,33]Charge-transfer salts such as CuTCNQ are a kind of high-performance organic materials which showed unique electrical properties and has been applied as optical and electrical recording media.[15,34−37] We expect that novel functions can be achieved by combining two semiconductors ZnO and CuTCNQ to form inorganic–organic p-n heterojunction hierarchical nanostructures. In this contribution, we develop a novel method of organic vapor-solid phase

Received: April 21, 2013
Accepted: May 30, 2013
Published: May 30, 2013

   dx.doi.org/10.1021/am4014677 | ACS Appl. Mater. Interfaces 2013, 5, 5825−5831

reaction to produce large-area 2D architectural CuTCNQ/ZnO nanotree (NT) arrays. The 2D architectural CuTCNQ/ZnO NT arrays display excellent diode nature, and the rectification ratios depend on the sizes of CuTCNQ NRs.

Up until now, the humidity sensors are mainly based on metal oxides or metal oxide hybrids[38−46] and the response or recovery of the sensors are usually conducted at high temperature. Furthermore, the detection limitation of the most common ZnO based humidity sensors in the literature can only reach 11% RH. In this work, a fast response/recovery diode-type humidity sensor based on the 2D architectural CuTCNQ/ZnO NT arrays has been first fabricated. The responding time of this humidity sensor is as fast as 60 s, and the detection limitation lowers to 5% RH at room temperature, which is better than that of other ZnO nanostructures.[47−53]

2. EXPERIMENTAL SECTION

Materials. TCNQ was purchased from Aldrich. Hexamine and zinc nitrate hexahydrate were obtained from Sinopharm Chemical Reagent Co. Ltd. All of the solvents were from Beijing Chemicals Corp. and used without further purification.

The ZnO NR arrays on the surface of indium tin oxide (ITO) glass (4× 4 cm^2) were prepared by the hydrothermal method.[54] The ZnO NR arrays were washed with deionized water and acetone and dried in the air before using. A layer of Cu was deposited on the surface of ZnO NR arrays by an ion sputter coater. The Cu layers with different thickness of 8 nm (sample A), 16 nm (sample B), 40 nm (sample C), and 70 nm (sample D), respectively, were obtained by controlling the sputtering time. After taken out, the ZnO NR arrays were coated with a layer of Cu and immediately protected by N_2 atmosphere to avoid oxidation by air. A porcelain boat containing 2 mg of TCNQ powders was placed in the center of the quartz tube, and the ZnO NR arrays substrate coated with a Cu layer was fixed 8 cm downstream. Then the quartz tube was inserted into a tube furnace and instantly heated to 170 °C under N_2 flow (20 standard cubic centimeters per minute). The temperature was maintained for 15 min. After taken out, the ZnO NR arrays turned deep green, which indicated the formation of CuTCNQ NRs (Scheme 1).

The hierarchical structure of CuTCNQ/ZnO NT arrays was characterized using scanning electron microscopy (SEM; Hitachi S4800 field emission scanning electron microscope) and transmission electron microscopy (TEM; JEOL JEM-2011). The characterization of CuTCNQ/ZnO was carried out by X-ray photoelectron spectroscopy (XPS; ESCAL ab220i-XL), X-ray diffraction (XRD; Rigaku D/max-2500), Fourier transform-infrared (FT-IR) spectroscopy (Biorad FTS6000), and Raman spectroscopy (DXR Raman Microscopy). The current−voltage (I−V) characteristics of the devices of CuTCNQ/ZnO were measured using a Keithley Semiconductor Characterization System (SCS-4200). For the humidity response test, the devices of CuTCNQ/ZnO NT arrays were put into the steel chamber filled with nitrogen of desired RH, which was connected with the Keithley Semiconductior Characterization System. In a typical humidity test, a pulse of air with desired RH was supplied to the chamber for 30 s, and then the steady-state current−voltage curve of the sensor was recorded. Subsequently, the humid air was pumped away and the nitrogen was supplied to the chamber and the recovery time was recorded. All these measurements were conducted at 25 °C. Furthermore, the effect of temperature on the humidity sensor was also studied. A pulse of 30% RH, which was obtained at 25 °C, was supplied to the chamber, then the steady-state current−voltage curves was recorded at different temperatures (10−70 °C).

3. RESULTS AND DISCUSSION

The hierarchical structure of CuTCNQ/ZnO NT arrays was prepared as follows (Scheme 1): The ZnO NR arrays on the surface of indium tin oxide (ITO) glass (4× 4 cm^2) were prepared by the hydrothermal method.[54] Then a layer of Cu

Scheme 1. Schematic Diagram of the Fabrication Process of CuTCNQ/ZnO NT Arrays[a]

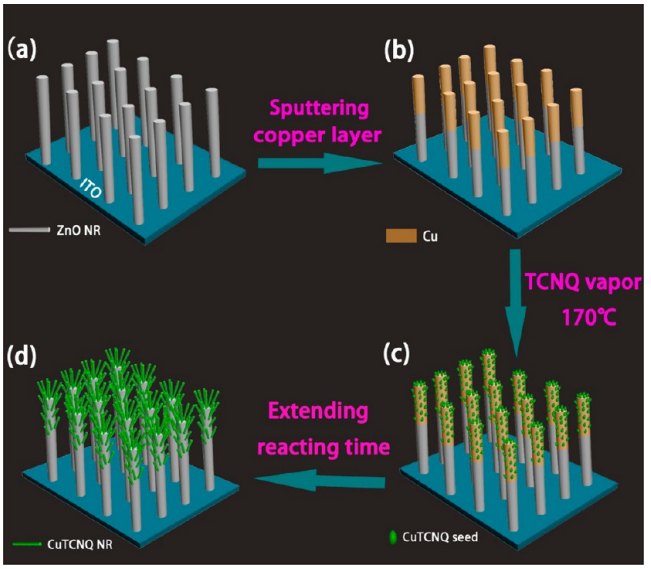

[a](a) The ZnO NR arrays align on the ITO substrate was prepared by hydrothermal method; (b) a layer of Cu was deposited on the ZnO NR arrays by sputtering; (c) the Cu reacted with TCNQ gas at high temperature to form CuTCNQ seeds; (d) CuTCNQ NRs were formed after 15 min reaction.

was deposited on the ZnO NR arrays, and the branched CuTCNQ NRs were grown by organic vapor solid phase reaction.[15] The as-prepared hierarchical structures of CuTCNQ/ZnO NT arrays were studied by FT-IR spectra, Raman spectra, and XPS spectra. The IR spectra of CuTCNQ/ZnO NT arrays show the typical absorptions of CuTCNQ (Figure 1a). The strong stretch of the CN group at 2202 cm^{-1}

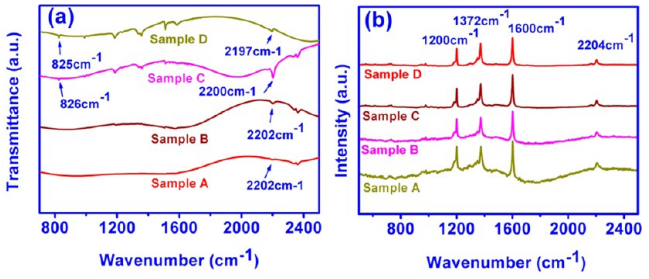

Figure 1. (a) FT-IR spectra of sample A, sample B, and sample D of CuTCNQ/ZnO NT arrays. For sample A and sample B, the CuTCNQ NR films were very thin, so the signals were weak and some peaks did not appear. The CuTCNQ NR film in sample D was much thicker thus resulting in strong signals and more peaks. (b) Raman spectra of sample A, sample B, and sample D of CuTCNQ/ZnO NT arrays.

with a shoulder at 2172 cm^{-1} displays that the CuTCNQ in CuTCNQ/ZnO NT arrays is phase I.[34−36] The peak at 826 cm^{-1} proves the presence of $TCNQ^-$,[34−36] which is very sensitive to change in the oxidation state. In Raman spectra of CuTCNQ/ZnO (Figure 1b), two characteristic principle vibration modes at 1372 cm^{-1} (C−CN wing stretching) and 2204 cm^{-1} (C−N stretching) are indicative of the existence of $TCNQ^-$.[34] As shown in the XPS spectra (Figure 2), the $2p^{3/2}$ and $2p^{1/2}$ signals (931.7 and 952 eV) exhibit essentially

dx.doi.org/10.1021/am4014677 | ACS Appl. Mater. Interfaces 2013, 5, 5825−5831

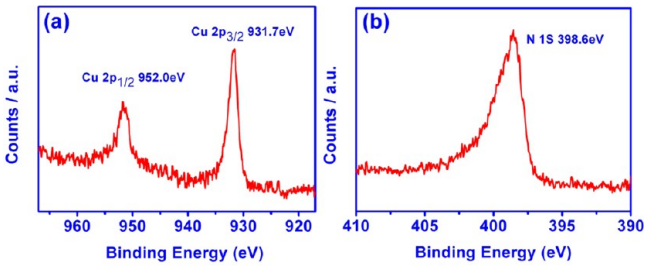

Figure 2. XPS data in the (a) Cu 2p and (b) N 1s regions of sample C of CuTCNQ/ZnO NT arrays.

identical binding energies for the Cu 2p orbital in accord with Cu(I).[35,36] The N 1s orbital appearing as a single feature at 398.6 eV is indicative of only one type of TCNQ in materials.[35,36] Figure S1 in the Supporting Information shows the XRD spectra of CuTCNQ/ZnO (sample C). For ZnO NR arrays, the XRD pattern is dominated by a strong peak of the (002) plane of wurtzite ZnO. For CuTCNQ/ZnO NT arrays, the characteristic peaks of phase I CuTCNQ appear at 16° and 25°, which are attributed to the (010) and (11-2) planes of CuTCNQ in CuTCNQ/ZnO NT arrays.[35,36]

As shown in Figure S2c in the Supporting Information, sample C (sputtering 32 nm thickness of Cu) on the ITO glass with a large area of 16 cm^2 is uniformly deep green film material, which is different from gray ZnO NR arrays (Figure S2a in the Supporting Information) and gray yellow ZnO NR coated with Cu layers (Figure S2b in the Supporting Information). Figure S3 in the Supporting Information shows that the ZnO NR arrays align on the ITO, and the diameter and length of the ZnO NRs are about 120 nm and 3 μm, respectively. The hierarchical structure of CuTCNQ/ZnO NT arrays have been confirmed by SEM and TEM. Figure 3 presents the SEM and TEM images of sample C. Figure 3a reveals that the deep green film on ITO consists of vertically growing hierarchical CuTCNQ/ZnO NT arrays, which are like nanotrees. The cross-section SEM image of the hierarchical CuTCNQ/ZnO NT arrays in Figure 3b shows that the oriented NTs are vertically aligned, in which ZnO NRs are backbones and CuTCNQ NRs are branches. The CuTCNQ NRs are nearly perpendicular with ZnO NRs. CuTCNQ NR only grows on the upper part of the ZnO nanorod. The inset in Figure 3a is a magnified SEM image of a typical single CuTCNQ/ZnO NT, in which the diameters and lengths of CuTCNQ NRs is about 40 and 200 nm, respectively. The TEM image of an individual CuTCNQ/ZnO NT in Figure 3c shows that the CuTCNQ/ZnO NT is well-defined, straight. Figure 3d,e are HRTEM images of the heterojunction areas at the top and side area of the CuTCNQ/ZnO NT, which are marked in Figure 3c. We can clearly observe the CuTCNQ/ZnO heterojunction formed between ZnO and CuTCNQ. The exact interface structure of the CuTCNQ/ZnO NT is observed, which indicates that the CuTCNQ attaches firmly on the single-crystalline ZnO. The lattice spacing around 0.26 nm observed in the images agrees well with the interplanar distance of the (002) direction parallel in the hexagonal wurtzite phase of ZnO.

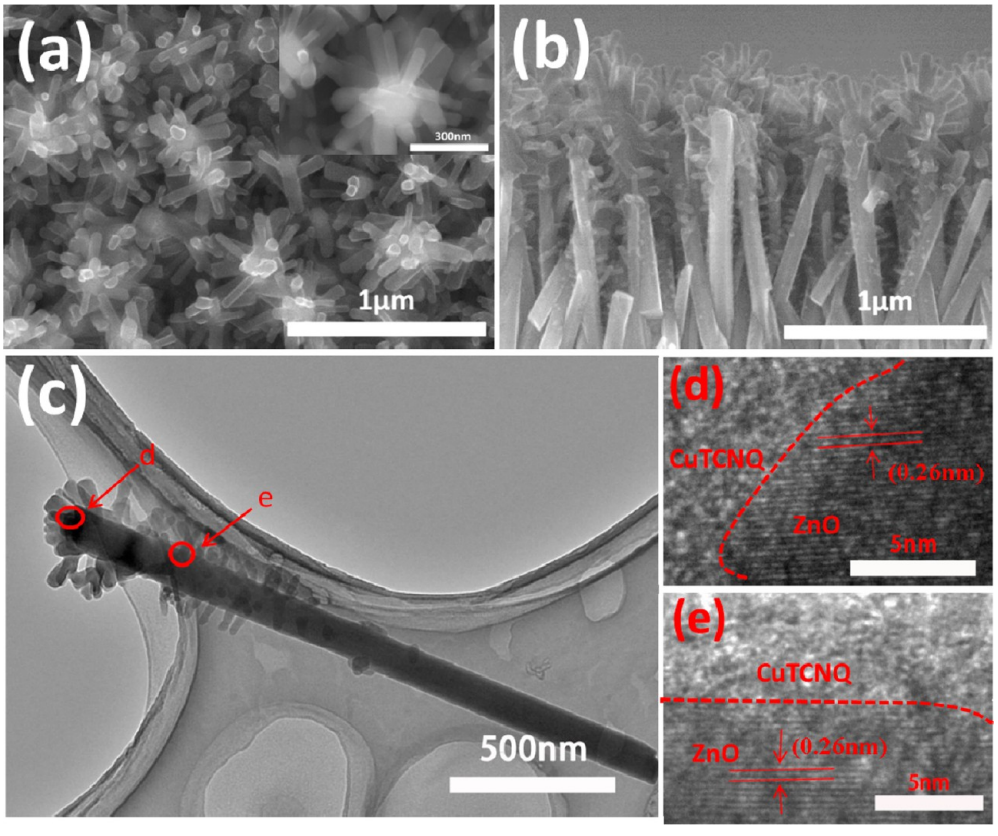

Figure 3. SEM images of sample C of CuTCNQ/ZnO NT arrays (a) top view, inset is the magnified top view; (b) the corresponding cross-section view; (c) TEM image of a an individual CuTCNQ/ZnO NT from sample C; (d and e) HRTEM images of the interface area between CuTCNQ NR and ZnO NR marked in part c.

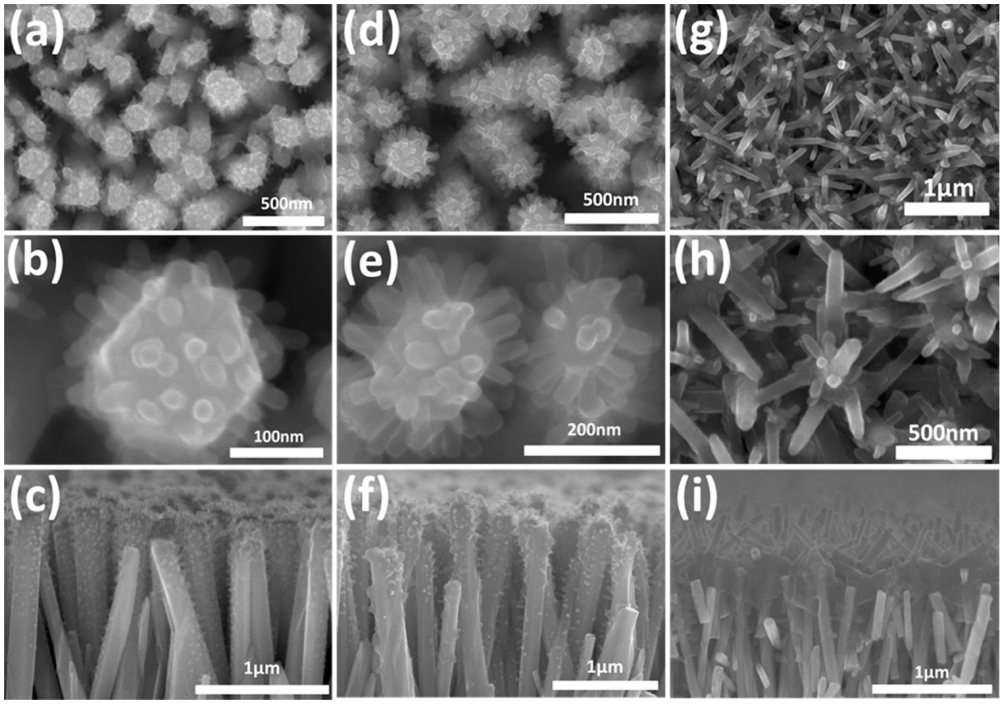

Figure 4. SEM images of top view (first row a, d, g), magnified top view (second row b, e, h), and the corresponding cross-section view (third row c, f, i) sample A (a–c), sample B (d–f), and sample D (g–i) of hierarchical structural CuTCNQ/ZnO NT arrays.

Figure 4 shows the top view and the corresponding cross-section view of other samples (A, B, and D) of CuTCNQ/ZnO NT arrays. The Cu source on the ZnO backbone was limited by the thickness of Cu layer, thus, the diameters and lengths of CuTCNQ NRs highly dependent on the thickness of the Cu layer. We can easily tune the diameters and lengths of CuTCNQ NRs in the growing process of CuTCNQ/ZnO NT arrays by controlling the thickness of the Cu layer. The diameter and length of CuTCNQ NRs in sample A (sputtering 8 nm thickness of Cu) is only 20 and 40 nm (Figure 4b) and increases to 100 and 500 nm in sample D (sputtering 72 nm thickness of Cu) (Figure 4h), respectively. Another interesting result is that the CuTCNQ NRs grown on each single ZnO NR show position-dependent sizes: CuTCNQ NRs on the sidewall are slightly smaller in both diameter and length than those growing at the top of the ZnO NR (Figures 3 and 4). This position-dependent nonuniformity of CuTCNQ NR growth is attributed to a nonuniform distribution of Cu during sputtering, in which the sidewall of ZnO NR will deposit less Cu than the top position per unit area. Moreover, the Cu layer could only coat about 1 μm of the the top of the ZnO NR owing to the shield effect by surrounding ZnO NRs. As a result, the root segment of the ZnO NR does not form CuTCNQ NRs. In other words, the size of branches of CuTCNQ/ZnO NT can be precisely controlled by tuning the thickness of the Cu layer.

All of the CuTCNQ/ZnO NT arrays were fabricated on the ITO as bottom electrodes, and a piece of Cu foil (0.5 × 0.5 cm^2) is placed on the top of CuTCNQ/ZnO NT arrays as the top electrode. Figure 5a shows typical $I-V$ characteristics of ITO/CuTCNQ/ZnO NT arrays/Cu devices, and obvious rectifying behaviors of a diode are observed for all samples. Rectification ratios (defined as the forward resistance divided by the reverse resistance) were calculated for all of the samples and listed in Table 1. Sample A shows the lowest rectification ratio (R) of 20.9 but rapidly increases to 57.5 for sample B and

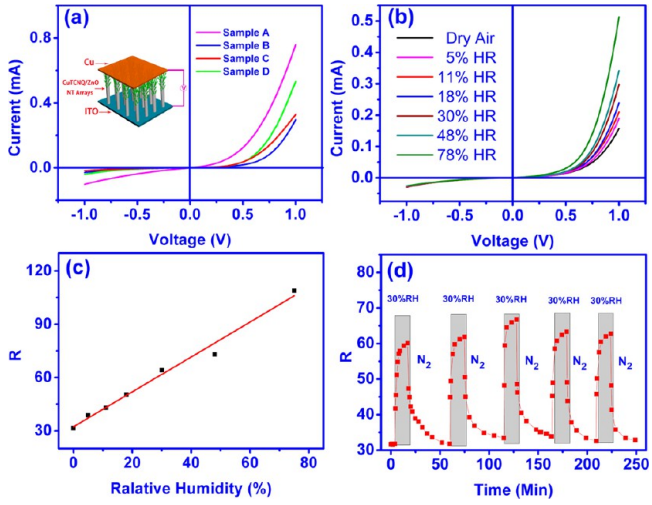

Figure 5. (a) $I-V$ characteristics of sample A, sample B, sample C, and sample D of CuTCNQ/ZnO NT arrays at room temperature, and the inset is the scheme of the ITO/CuTCNQ/ZnO NT arrays/Cu device; (b) $I-V$ characteristics of sample B measured at at 25 °C exposed to different RH; (c) calculated R of sample B as a function of RH; (d) R response of sample B between dry pure nitrogen and 30% RH.

Table 1. Rectification Ratios (R), Ideality Factor (n), and Saturation Current (I_{sat}) of CuTCNQ/ZnO NT Arrays (Samples A–D)

	sample A	sample B	sample C	sample D
R	20.9	57.5	86.9	89.8
n	2.96	2.20	2.48	3.02
I_{sat} (μA)	4.12	1.24	0.23	0.92

86.9 for sample C. For sample D, the R reaches the maximum value of 89.8. The R values of CuTCNQ/ZnO NRs NT arrays

dx.doi.org/10.1021/am4014677 | ACS Appl. Mater. Interfaces 2013, 5, 5825–5831

are morphology-dependent. It is well-known that the surface leakage current is an important factor in the determination of reverse current and the rectification ratio. For sample A (Figure 4a–c), the short and neat CuTCNQ NRs on the top of ZnO NR will result in a larger contact area when connected with the Cu foil electrode, which will bring about a large surface leakage current and lead to a large reverse saturation current and small rectification ratios. For sample B (Figure 4d–f), sample C (Figure 3a), and sample D (Figure 4g–i), the longer and differently oriented CuTCNQ NRs will lead to a smaller contact area with the Cu electrode, resulting in smaller surface leakage current and higher rectification ratios.

The current–voltage response of these diodes is modeled using the ideal diode equation: $I = I_{sat} \exp(eV/nkT) - 1$,[55] where e is the electronic charge, V is the applied voltage, k is the Boltzmann constant, n is the ideality factor, and I_{sat} is the reverse saturation current. This equation is used to describe the behavior of a single p-n junction. The CuTCNQ/ZnO NT arrays are composed of many p-n junctions, and thus the overall $I-V$ measurement will be a total of these characteristics. In the linear region, the ideal diode equation can be written as: $\ln I = eV/nkT + \ln I_{sat}$. The slope and intercept of the fitted line to the linear region give the values of n and I_{sat}. The ideality factor n is a figure of merit that describes the recombination behavior of the device. A device governed purely by diffusion current will have $n = 1$ (ideal diode), while a device dominated by recombination will have $n = 2$. The values of n (0.05 V < V < 0.15 V) for CuTCNQ/ZnO NT arrays were calculated and listed in Table 1. The ideality factors for the CuTCNQ/ZnO NT arrays are slightly greater than 2, which means the CuTCNQ/ZnO diodes are a nearly ideal diode governed by recombination, better than those ZnO-based p-n diodes reported.[56] The ideality of the diodes is attributed to the high quality of the CuTCNQ/ZnO p-n heterojunction formed through the coordination interactions between cyano groups of CuTCNQ and zinc ions of ZnO and the interactions between copper ions of CuTCNQ and oxygen ions of ZnO. Another factor that will reduce the ideality is the adsorbed oxygen on the surface of ZnO. The chemisorbed oxygen can capture free electrons from the conduction band of ZnO NRs and form oxygen ions (O^{2-}), creating a new depletion layer at the interface of ZnO and CuTCNQ and resulting in a low diffusion current.[56] In the growing CuTCNQ/ZnO NT arrays, the adsorbed oxygen can be easily replaced by the coordination of cyano groups of CuTCNQ. The reverse saturation current I_{sat}, which measures how many carriers can overcome the energetic barrier created by the p-n junction in the reverse bias direction, is another factor that determines the behavior of a diode.[55] It should minimize the I_{sat} to improve overall rectification of the device. The I_{sat} of CuTCNQ/ZnO NT arrays were calculated and listed in Table 1, all of which are less than 5 μA and with a minimum value of 0.23 μA for sample C.

From the results of $I-V$ performances in Figure 5a, the forward currents of CuTCNQ/ZnO NT diodes are not consistent with each other. These results can be explained by the variation of morphology of the CuTCNQ NRs. According to the resistance formula, longer CuTCNQ NRs lead to higher resistance. From sample A to sample B, the device resistance decreases with elongating of the CuTCNQ NRs when their diameter does not change too much. However, in sample C and sample D, the diameters of CuTCNQ NRs get much thicker (Figure 4i), which offsets the effect of length increase, thus the resistances decrease compared with sample B.

A variety of humidity sensors have been developed based on metal oxide nanostructures,[38−46] but they are almost the general electrical resistance detection mode. As a diode, its basic characteristic will amplify the electrical signal. So it is very interesting to design a diode-type humidity sensor using CuTCNQ/ZnO NT arrays because of its excellent diode nature. In addition, the 2D architecture possesses a large surface area because of its peculiar branching structure, which would enhance molecular contact and transport kinetics. Indeed, the humidity sensor fabricated from the 2D architectural CuTCNQ/ZnO NT arrays exhibited ultrahigh sensitivity and quick response and recovery at room temperature. Sample B was selected to make all of the response measurement due to its ideality factor $n = 2.20$, which means an ideal diode. As depicted in Figure 5b, the forward current of sample B increased triply with the increase of humidity while the reverse current was almost constant. A response down to 5% RH can be reached, which is lower than humidity sensors of ZnO nanostructrues reported.[47−53] Corresponding R (rectification ratios) values of 2D architectural CuTCNQ/ZnO NT arrays exposed to different RHs were calculated according to the definition of R discussed above and were shown in Figure 5c. The values of R have a nearly linear relation with RH, which indicates that the RH could be quantitatively detected. Pulses of humidity air (nitrogen saturated with water vapor) and pure dry nitrogen were injected into the chamber, and transient responses were recorded to check the response, recovery, and repeatability of the device, as shown in Figure 5d. Five circles of measurements were performed to show the good reproducibility of the humidity sensor. The response to humidity at different temperatures was also studied. Under 30% RH at 10 °C, the forward current of the sensor increased doubly, but the current changed little when the temperature increased from 10 to 70 °C (Figure S7 in the Supporting Information). This result proved the conductivity of ZnO and CuTCNQ in this temperature range is nearly constant. Therefore, the sensor has been demonstrated to work well without the effect of temperature at moderate temperatures.

The response (defined as reaching 80% of the maximum value) and recovery (defined as reaching the original value) times of CuTCNQ/ZnO NT arrays humidity sensor are about 60 s and 30 min, respectively. Significantly, the limitation of detection reaches 5% HR, which is lower than other ZnO-based humidity sensors reported previously.[47−53] Both the detection and regeneration of the sensor were conducted at room temperature (25 °C). The range of humidity response is 5–75% HR (25 °C), which is also wider than most of other ZnO humidity sensors.[47−53] An ionic conduction mechanism has been demonstrated for ZnO and TiO_2 based humidity sensors.[49,57] Because CuTCNQ nanostructures did not present response to humidity, the ionic conduction mechanism is also fitted for CuTCNQ/ZnO NT arrays humidity sensor. In this mechanism, surface activity is a key factor determining the proton concentration. For the CuTCNQ/ZnO NT arrays humidity sensor, the excellent sensing performance profits from the large heterojunction interface area between ZnO and CuTCNQ, which induces more defects for available oxygen vacancies on the surface of ZnO NR. Thus, the surface activity of ZnO is promoted. In the samples, when exposed to a humid vapor, the surface of ZnO NRs will physically adsorb water molecules in place of the previous chemisorbed oxygen molecules. Then the protons dissociated from water molecules act as charge carriers for transporting charge between

physisorbed water molecules on the ZnO surface. The increase of free protons leads to the increase of forward conductivity.[58]

4. CONCLUSIONS

In summary, we have developed a strategy of organic vapor solid phase reaction for controlled growing of large-area (16 cm^2) 2D ordered aligned inorganic−organic p-n heterojunction CuTCNQ/ZnO NT arrays. The sizes of the branched CuTCNQ NRs can be precisely tuned by changing the thickness of Cu sputtering on the ZnO NR backbone. Increasing the thickness of the Cu layer can result in increased lengths and diameters of CuTCNQ NRs. The CuTCNQ/ZnO NT arrays show a perfect diode feature and exhibit obvious size-dependent rectification ratios. In particular, CuTCNQ/ZnO NT with a large heterojunction interface area possesses more available oxygen vacancies on the surface of ZnO NR, which induces a higher surface activity of ZnO. The p-n heterojunction arrays exhibit an ultrahigh sensitivity for detecting humidity at 25 °C. The limit of response is low to 5% RH, along with a fast response and recovery at 25 °C. The present work provides a novel method for the controlled synthesis of large-area inorganic−organic heterojunction multihierarchical nanostructures and opens a new way for the fabrication of diode-type sensors based on a strong p-n heterojunction effect.

■ ASSOCIATED CONTENT

Supporting Information

XRD pattern, XPS results analysis, more SEM and TEM images, current−voltage data, and photographs of CuTCNQ/ZnO NT arrays. This material is available free of charge via the Internet at http://pubs.acs.org.

■ AUTHOR INFORMATION

Corresponding Author

*E-mail: liuhb@iccas.ac.cn.

Notes

The authors declare no competing financial interest.

■ ACKNOWLEDGMENTS

This study was supported by the National Basic Research 973 Program of China (Grants 2011CB932302 and 2012CD932900) and the National Nature Science Foundation of China (Grants 21031006, 90922007, and 21290190).

■ ABBREVIATIONS

NT, nanotrees
NR, nanorod
TCNQ, 7,7,8,8-tetracyanoquinodimethane
RH, relative humidity
R, rectification ratio

■ REFERENCES

(1) Robinson, J. T.; Jorgolli, M.; Shalek, A. K.; Yoon, M. H.; Gertner, R. S.; Park, H. *Nat. Nanotechnol.* **2012**, *7*, 180−184.
(2) Benson, J.; Boukhalfa, S.; Magasinski, A.; Kvit, A.; Yushin, G. *ACS Nano* **2011**, *6*, 118−125.
(3) Breuer, S.; Pfüller, C.; Flissikowski, T.; Brandt, O.; Grahn, H. T.; Geelhaar, L.; Riechert, H. *Nano Lett.* **2011**, *11*, 1276−1279.
(4) Cui, S.; Liu, H. B.; Gan, L. B.; Li, Y. L.; Zhu, D. B. *Adv. Mater.* **2008**, *20*, 2918−2925.
(5) Liu, H. B.; Xu, J. l.; Li, Y. J.; Li, Y. J. *Acc. Chem. Res.* **2010**, *43*, 1496−1508.
(6) Qin, Y.; Wang, X. D.; Wang, Z. L. *Nature* **2008**, *451*, 809−813.
(7) Rauber, M.; Alber, I.; Müller, S.; Neumann, R.; Picht, O.; Roth, C.; Schökel, A.; Toimil-Molares, M. E.; Ensinger, W. *Nano Lett.* **2011**, *11*, 2304−2310.
(8) Wang, Z. L.; Song, J. H. *Science* **2006**, *312*, 242−246.
(9) Song, J. H.; Wang, X. D.; Liu, J.; Liu, H. B.; Li, Y. L.; Wang, Z. L. *Nano Lett.* **2007**, *8*, 203−207.
(10) Xu, S.; Qin, Y.; Xu, C.; Wei, Y. G.; Yang, R. S.; Wang, Z. L. *Nat. Nanotechnol.* **2010**, *5*, 366−373.
(11) Cui, S.; Li, Y. L.; Guo, Y. B.; Liu, H. B.; Song, Y. L.; Xu, J. L.; Lv, J.; Zhu, M.; Zhu, D. B. *Adv. Mater.* **2008**, *20*, 309−313.
(12) Gan, H. Y.; Liu, H. B.; Li, Y. J.; Zhao, Q.; Li, Y. L.; Wang, S.; Jiu, T. G.; Wang, N.; He, X. R.; Yu, D. P.; Zhu, D. B. *J. Am. Chem. Soc.* **2005**, *127*, 12452−12453.
(13) Huang, C. S.; Li, Y. L.; Song, Y. L.; Li, Y. J.; Liu, H. B.; Zhu, D. B. *Adv. Mater.* **2010**, *22*, 3532−3536.
(14) Huang, C. S.; Wen, L. P.; Liu, H. B.; Li, Y. L.; Liu, X. F.; Yuan, M. J.; Zhai, J.; Jiang, L.; Zhu, D. B. *Adv. Mater.* **2009**, *21*, 1721−1725.
(15) Liu, H. B.; Zhao, Q.; Li, Y. L.; Liu, Y.; Lu, F. S.; Zhuang, J. P.; Wang, S.; Jiang, L.; Zhu, D. B.; Yu, D. P.; Chi, L. F. *J. Am. Chem. Soc.* **2005**, *127*, 1120−1121.
(16) Zhao, Y. S.; Fu, H. B.; Hu, F. Q.; Peng, A. D.; Yang, W. S.; Yao, J. N. *Adv. Mater.* **2008**, *20*, 79−83.
(17) Zhao, Y. S.; Fu, H. B.; Peng, A. D.; Ma, Y.; Liao, Q.; Yao, J. N. *Acc. Chem. Res.* **2009**, *43*, 409−418.
(18) Xiao, J.; Yang, B.; Wong, J. I.; Liu, Y.; Wei, F.; Tan, K. J.; Teng, X.; Wu, Y.; Huang, L.; Kloc, C.; Boey, F.; Ma, J.; Zhang, H.; Yang, H. Y.; Zhang, Q. *Org. Lett.* **2011**, *13*, 3004−3007.
(19) Xiao, J.; Yang, H.; Yin, Z.; Guo, J.; Boey, F.; Zhang, H.; Zhang, Q. *J. Mater. Chem.* **2011**, *21*, 1423−1427.
(20) Xiao, J.; Yin, Z.; Li, H.; Zhang, Q.; Boey, F.; Zhang, H.; Zhang, Q. *J. Am. Chem. Soc.* **2010**, *132*, 6926−6928.
(21) Xiao, J.; Yin, Z.; Wu, Y.; Guo, J.; Cheng, Y.; Li, H.; Huang, Y.; Zhang, Q.; Ma, J.; Boey, F.; Zhang, H.; Zhang, Q. *Small* **2011**, *7*, 1242−1246.
(22) Yang, B.; Xiao, J.; Wong, J. I.; Guo, J.; Wu, Y.; Ong, L.; Lao, L. L.; Boey, F.; Zhang, H.; Yang, H. Y.; Zhang, Q. *J. Phys. Chem. C* **2011**, *115*, 7924−7927.
(23) Zhao, J.; Wong, J. I.; Wang, C.; Gao, J.; Ng, V. Z. Y.; Yang, H. Y.; Loo, S. C. J.; Zhang, Q. *Chem. Asian J.* **2013**, *8*, 665−669.
(24) Liu, H. B.; Zuo, Z. C.; Guo, Y.; Li, Y.; Li, Y. *Angew. Chem., Int. Ed.* **2010**, *49*, 2705−2707.
(25) Chen, N.; Qian, X. M.; Lin, H. W.; Liu, H. B.; Li, Y. J.; Li, Y. L. *Dalton Trans.* **2011**, *40*, 10804−10808.
(26) Guo, Y. B.; Liu, H. B.; Li, Y. J.; Li, G. X.; Zhao, Y. J.; Song, Y. L.; Li, Y. L. *J. Phys. Chem. C* **2009**, *113*, 12669−12673.
(27) Guo, Y. B.; Tang, Q. X.; Liu, H. B.; Zhang, Y. J.; Li, Y. L.; Hu, W. P.; Wang, S.; Zhu, D. B. *J. Am. Chem. Soc.* **2008**, *130*, 9198−9199.
(28) Lin, Y. Y.; Chu, T. H.; Li, S. S.; Chuang, C. H.; Chang, C. H.; Su, W. F.; Chang, C. P.; Chu, M. W.; Chen, C. W. *J. Am. Chem. Soc.* **2009**, *131*, 3644−3649.
(29) Liu, H. B.; Cui, S.; Guo, Y. B.; Li, Y. L.; Huang, C. S.; Zuo, Z. C.; Yin, X. D.; Song, Y. L.; Zhu, D. B. *J. Mater. Chem.* **2009**, *19*, 1031−1036.
(30) Haberkorn, N.; Gutmann, J. S.; Theato, P. *ACS Nano* **2009**, *3*, 1415−1422.
(31) Liu, H. B.; Li, Y. L.; Jiang, L.; Luo, H. Y.; Xiao, S. Q.; Fang, H. J.; Li, H. M.; Zhu, D. B.; Yu, D. P.; Xu, J.; Xiang, B. *J. Am. Chem. Soc.* **2002**, *124*, 13370−13371.
(32) He, J. H.; Lao, C. S.; Chen, L. J.; Davidovic, D.; Wang, Z. L. *J. Am. Chem. Soc.* **2005**, *127*, 16376−16377.
(33) Huang, M. H.; Mao, S.; Feick, H.; Yan, H. Q.; Wu, Y. Y.; Kind, H.; Weber, E.; Russo, R.; Yang, P. D. *Science* **2001**, *292*, 1897−1899.
(34) Pearson, A.; O'Mullane, A. P.; Bansal, V.; Bhargava, S. K. *Inorg. Chem* **2011**, *50*, 1705−1712.
(35) Heintz, R. A.; Zhao, H. H.; Xiang, O. Y.; Grandinetti, G.; Cowen, J.; Dunbar, K. R. *Inorg. Chem* **1999**, *38*, 144−156.
(36) Neufeld, A. K.; Madsen, I.; Bond, A. M.; Hogan, C. F. *Chem. Mater.* **2003**, *15*, 3573−3585.

(37) Chen, X.; Zheng, G.; Cutler, J. I.; Jang, J.-W.; Mirkin, C. A. *Small* **2009**, *5*, 1527−1530.
(38) Arshak, K. I.; Twomey, K. *Microelectron. J.* **2002**, *33*, 213−220.
(39) Wolfbeis, O. S. *Anal. Chem.* **2004**, *76*, 3269−3284.
(40) Chen, Z.; Lu, C. *Sens. Lett.* **2005**, *3*, 274−295.
(41) Kuang, Q.; Lao, C.; Wang, Z. L.; Xie, Z.; Zheng, L. *J. Am. Chem. Soc.* **2007**, *129*, 6070−6071.
(42) Li, Z.; Zhang, H.; Zheng, W.; Wang, W.; Huang, H.; Wang, C.; MacDiarmid, A. G.; Wei, Y. *J. Am. Chem. Soc.* **2008**, *130*, 5036−5037.
(43) Wang, Z.; Zhang, J.; Xie, J.; Li, C.; Li, Y.; Liang, S.; Tian, Z.; Wang, T.; Zhang, H.; Li, H.; Xu, W.; Yang, B. *Adv. Funct. Mater.* **2010**, *20*, 3784−3790.
(44) Hawkeye, M. M.; Brett, M. J. *Adv. Funct. Mater.* **2011**, *21*, 3652−3658.
(45) Liu, K.; Sakurai, M.; Aono, M. *Small* **2012**, *8*, 3599−3604.
(46) Zhang, Y.; Chen, Y.; Zhang, Y.; Cheng, X.; Feng, C.; Chen, L.; Zhou, J.; Ruan, S. *Sens. Actuators, B* **2012**, *174*, 485−489.
(47) Hu, X.; Gong, J.; Zhang, L.; Yu, J. C. *Adv. Mater.* **2008**, *20*, 4845−4850.
(48) Qi, Q.; Zhang, T.; Zeng, Y.; Yang, H. B. *Sens. Actuators, B* **2009**, *137*, 21−26.
(49) Qiu, Y.; Yang, S. *Adv. Funct. Mater.* **2007**, *17*, 1345−1352.
(50) Raj, A.; Magdalane, C. M.; Nagaraja, K. S. *Phys. Status Solidi A* **2002**, *191*, 230−234.
(51) Wang, X. H.; Ding, Y. F.; Zhang, J.; Zhu, Z. Q.; You, S. Z.; Chen, S. Q.; Zhu, J. Z. *Sens. Actuators, B* **2006**, *115*, 421−427.
(52) Zainelabdin, A.; Amin, G.; Zaman, S.; Nur, O.; Lu, J.; Hultman, L.; Willander, M. *J. Mater. Chem.* **2012**, *22*, 11583−11590.
(53) Zhang, Y. S.; Yu, K.; Jiang, D. S.; Zhu, Z. Q.; Geng, H. R.; Luo, L. Q. *Appl. Surf. Sci.* **2005**, *242*, 212−217.
(54) Qian, X. M.; Liu, H. B.; Guo, Y. B.; Song, Y. L.; Li, Y. J. *Nanoscale Res. Lett.* **2008**, *3*, 303−307.
(55) Novotny, C. J.; Yu, E. T.; Yu, P. K. L. *Nano Lett.* **2008**, *8*, 775−779.
(56) Tang, Q. W.; Lin, L.; Zhao, X.; Huang, K.; Wu, J. H. *Langmuir* **2012**, *28*, 3972−3978.
(57) Schaub, R.; Thostrup, P.; Lopez, N.; Lægsgaard, E.; Stensgaard, I.; Nørskov, J. K.; Besenbacher, F. *Phys. Rev. Lett.* **2001**, *87*, 266104−266107.
(58) Kiasari, N. M.; Soltanian, S.; Gholamkhass, B.; Servati, P. *Sens. Actuators, A* **2012**, *182*, 101−105.